

# High-precision Carrier Tracking Algorithm for extremely Weak and High-Dynamic Signal

Tao Deng<sup>1</sup>, Maoli Ma<sup>2</sup>, Qinghui Liu<sup>1</sup>, and Yajun Wu<sup>3</sup>

<sup>1</sup>Shanghai Astronomical Observatory, Chinese Academy of Sciences

<sup>2</sup>Shanghai Astronomical Observatory

<sup>3</sup>SHAO

November 22, 2022

## Abstract

Obtaining high-precision Doppler frequency for very weak signals in deep space exploration is challenging. A phase-locked loop (PLL) is a widely used high-precision Doppler frequency measurement method, and the arctangent phase detector is the most widely used phase detector. However, the arctangent phase detector cannot correctly identify the signal phase for signals with very low signal-to-noise ratio (SNR) and very high dynamic. Therefore, the arctangent phase detector is the key module limiting the weak-signal and high-dynamic tracking abilities of a PLL. This study proposes a new phase discrimination method in which the phase difference between the real and the reconstructed signals is obtained by using the coefficients of signal transformation. By replacing arctangent phase detector with novel phase detector, the high-dynamic and weak-signal tracking abilities of PLL are greatly improved. This method is expected to provide a good reference for radar, navigation, and other fields involving carrier tracking, and it provides feasible technical solutions for high-precision carrier tracking of high-dynamic and low-SNR signals on some occasions.

# High-precision Carrier Tracking Algorithm for extremely Weak and High-Dynamic Signal

Tao Deng<sup>1,2</sup>, Maoli Ma<sup>1</sup>, Qinghui Liu<sup>1</sup>, Yajun Wu<sup>1</sup>

<sup>1</sup>Shanghai Astronomical Observatory, Chinese Academy of Sciences, Shanghai 200030, China

<sup>2</sup>University of Chinese Academy of Sciences, Beijing 100049, China

## Key Points:

- Obtaining high-precision Doppler frequency for high-dynamic and very weak signals in deep space exploration is challenging.
- By replacing the arctangent phase detector with novel phase detector, the performances of PLL are greatly improved, including the high-dynamic and weak-signal tracking ability, tracking accuracy.
- The new proposed method is suitable for carrier tracking in deep space exploration, especially when large dynamic is contained in signals.

---

Corresponding author: Tao Deng; Qinghui Liu, [dengtao@shao.ac.cn](mailto:dengtao@shao.ac.cn); [liuqinghui@shao.ac.cn](mailto:liuqinghui@shao.ac.cn)

## Abstract

Obtaining high-precision Doppler frequency for very weak signals in deep space exploration is challenging. A phase-locked loop (PLL) is a widely used high-precision Doppler frequency measurement method, and the arctangent phase detector is the most widely used phase detector. However, the arctangent phase detector cannot correctly identify the signal phase for signals with very low signal-to-noise ratio (SNR) and very high dynamic. Therefore, the arctangent phase detector is the key module limiting the weak-signal and high-dynamic tracking abilities of a PLL. This study proposes a new phase discrimination method in which the phase difference between the real and the reconstructed signals is obtained by using the coefficients of signal transformation. By replacing arctangent phase detector with novel phase detector, the high-dynamic and weak-signal tracking abilities of PLL are greatly improved. This method is expected to provide a good reference for radar, navigation, and other fields involving carrier tracking, and it provides feasible technical solutions for high-precision carrier tracking of high-dynamic and low-SNR signals on some occasions.

## 1 Introduction

In deep space exploration, the signals received by ground stations are often very weak and contain a large dynamic Doppler effect. Consider the examples of the Mars Exploration Rover (MER) missions MER-A and MER-B : in the entry, descent, and landing (EDL) phase, the range of the first and second derivatives of the Doppler frequency is  $0 \sim 1200 Hz/s$  and around  $-25 Hz/s^2 \sim 40 Hz/s^2$ , respectively (Satorius et al., 2003). The first derivative of the Curiosity probe's Doppler frequency is even close to  $3500 Hz/s$  (Soriano et al., 2012; Hao et al., 2018). At the same time, the signals received by the ground stations are very weak. For signals of the Curiosity probes EDL phase received by the 70-m antenna, the carrier-to-noise ratio (CNR) is around  $27 dB-Hz$  under normal conditions (Hao et al., 2018). During the Jupiter probe's Jupiter orbital insertion (JOI) phase, the CNR of the signal received by the ground station was as low as  $12 \sim 15 dB-Hz$  (Soriano et al., 2012). These observations indicate that high-precision tracking of signals with very low signal-to-noise ratio (SNR) or high dynamic is one of the focal problems in communication for deep space exploration. This problem also applies to other application fields involving carrier tracking, such as a global navigation satellite system (GNSS) receiver: the satellite signal received by the receiver is very weak under the action of some natural or artificial factors. Therefore, it is also essential to develop a corresponding high-sensitivity and high-precision carrier tracking algorithm.

For estimating the Doppler frequency in Mars rover's EDL phase, one method compensated a series of phases for the original signal in the time domain and then detected the compensation value corresponding to the maximum energy to determine the Doppler frequency (Satorius et al., 2003). Maximum likelihood estimation is also a feasible method for carrier tracking in EDL phase (Cattivelli et al., 2008). However, the both methods are open-loop methods which require considerable computational resources to realize real-time processing, especially when sampling rate of data is large. Further, since only linear frequency model is considered, these two methods have limited tracking accuracy. Another study proposed an adaptive linear prediction method (ALP) to estimate the Doppler frequency (Lopes et al., 2006). Compared with the method proposed in (Satorius et al., 2003), ALP requires significantly lesser computational resources; however, its tracking accuracy remains inadequate.

A frequency-locked loop (FLL) based on a fast Fourier transform (FFT) frequency discriminator has a strong ability to track a weak signal. However, the FFT frequency discriminator has low frequency resolution, resulting in low tracking accuracy of Doppler frequency. Furthermore, the dynamic tracking ability is restricted by the characteristics of the FFT frequency discriminator itself.

A phase-locked loop (PLL) is a high-precision Doppler frequency tracking algorithm. Phase-locked loop (PLL) architectures are still widely used in many modern receivers. How-

65 ever, a traditional PLL is seriously compromised by many factors, including high dynamics,  
 66 shadowing, strong fadings and so on(Vila-Valls et al., 2017).

67 Therefore, many PLL improvement strategies have been proposed. One is to combine  
 68 the FLL with the PLL; doing so combines the high-dynamic tracking capability of the FLL  
 69 with the high-precision tracking capability of the PLL(Mao & Chen, 2008). The tracking  
 70 accuracy and weak-signal tracking ability of the PLL can also be improved by adopting  
 71 Kalman filters (KF)(Won et al., 2012). Furthermore, adaptive KFs (AKFs) provide robust  
 72 solutions compared with KFs(Vil-Valls et al., 2015; Won, 2014). It is also feasible to com-  
 73 bine wavelet packet denoising with a PLL to improve the tracking accuracy or weak-signal  
 74 tracking ability of a PLL(Li et al., 2011). In addition, discrete wavelet transform filtering  
 75 and Kalman filters(KF) are combined to enhance signal carrier tracking robustness(Ruan  
 76 et al., 2017).Wavelet de-noising adaptive Kalman filter (AKF) are also presented in Sun et  
 77 al. (2017); Pengyue et al. (2016).

78 In this study, the phase discriminator is recognized as a key module that limits PLL  
 79 performance improvement, and a new phase discriminator is designed by signal transforma-  
 80 tion which basis function is new defined. The novel phase detector is used to replace the  
 81 traditional arctangent phase detector, resulting in a large improvement in the PLL perfor-  
 82 mance. This improvement enables accurate estimation of Doppler frequency of extremely  
 83 weak and high-dynamic signals.

## 84 2 Realization of novel phase detector

### 85 2.1 The structure of Costas PLL

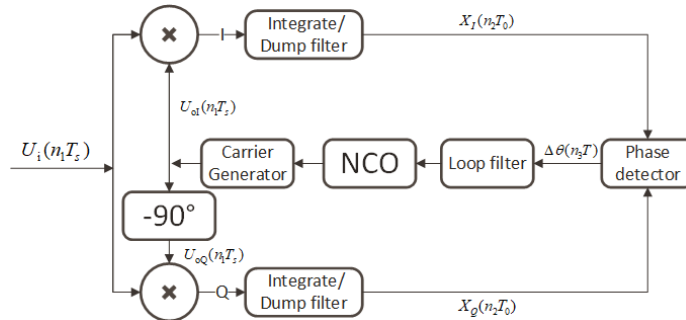


Figure 1. Costas PLL structure.

86 Figure 1 shows the structure of the PLL. The input signal and the reconstructed sig-  
 87 nals of the two branches are respectively mixed, and then, the mixed signals are sent to  
 88 integrate/dump filter. Integrate/dump filter is a low pass filter. We assume that the period  
 89 used in integrate/dump filter in figure 1 is  $T_0$ , and the function is summing up the data for  
 90 each continuous period of time( $T_0$ ). The phase difference between the real and the recon-  
 91 structed signals can be identified by phase detector. The phase detector's output is used as  
 92 the input of the loop filter (LPF). NCO is an integrator. Finally, the NCO's output is used  
 93 to generate the reconstructed signal.

94 Figure 2 shows the linear discrete structure of a third-order Costas PLL. The transfor-  
 95 mation between a continuous system and a discrete system is given by

$$96 \quad \frac{1}{s} = \frac{Tz^{-1}}{1 - z^{-1}}. \quad (1)$$

97 The measured Doppler frequency is

$$98 \quad f_1 = \frac{w_1}{2\pi T}. \quad (2)$$

99 As is seen in figure 2, loop filter is JR(Jaffe-Rechtin) filter(Tian et al., 2016),  $w_1$  is the  
100 output of JR filter.  $T$  is sampling period of input data of JR filter.  $\omega_n$  is natural frequency  
101 of PLL.

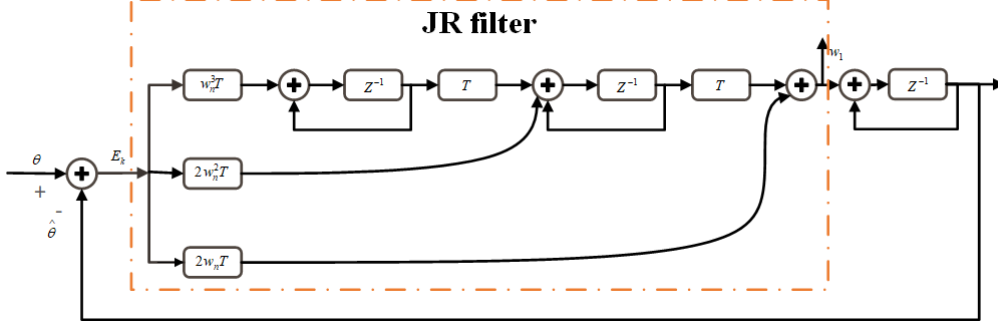


Figure 2. Linear discrete structure of third-order Costas PLL.

## 102 2.2 Basic principle of novel phase detector

103 Wavelet transform is suitable for signal denoising by decomposing signal and noise into  
104 different spaces. In the field of optics, wavelet transform can be used for phase retrieval from  
105 fringe pattern(Zhong & Weng, 2005). Similar to wavelet function used in wavelet transform,  
106 a new basis function is defined and which is given by

$$107 \quad \psi(t) = \left(\frac{1}{R} - \frac{t^2}{R^2}\right) \exp\left(-\frac{t^2}{2R^2}\right) \quad (3)$$

108 In equation (3),  $R$  is an adjustable parameter. In a practical application,  $R$  would be set to  
109 a fixed constant.

110 When  $R = 1$ ,  $\psi(t)$  is known as Mexican hat wavelet, and the admissibility condition is  
111 satisfied. When  $R \neq 1$ , the admissibility condition is not satisfied, that is, the  $\psi(t)$  does not  
112 satisfy

$$113 \quad C_\psi = \int_{-\infty}^{\infty} \frac{|\widehat{\psi}(\omega)|^2}{|\omega|} d\omega < +\infty \quad (4)$$

114  $\widehat{\psi}(\omega)$  is Fourier transform of  $\psi(t)$ . It means that when  $R \neq 1$ ,  $\psi(t)$  isn't a wavelet func-  
115 tion because the traditional definition of wavelet requires that it satisfies the admissibility  
116 condition. But  $\psi(t)$  can be still a basis function used in signal transformation.

117 The Fourier transform of equation (3) is

$$118 \quad \widehat{\psi}(\omega) = \sqrt{2\pi} (1 - R + R^3 \omega^2) \exp\left(-\frac{1}{2} R^2 \omega^2\right). \quad (5)$$

119  $\widehat{\psi}(\omega)$  is shown in Figure 3. When the frequency exceeds a certain range, the amplitude  
120 rapidly decays to close to 0.

121 Just like family of wavelets defined in wavelet analysis, the corresponding family of  $\psi(t)$   
122 is

$$123 \quad \psi_{a,b}(t) = \frac{1}{\sqrt{a}} \psi\left(\frac{t-b}{a}\right). \quad (6)$$

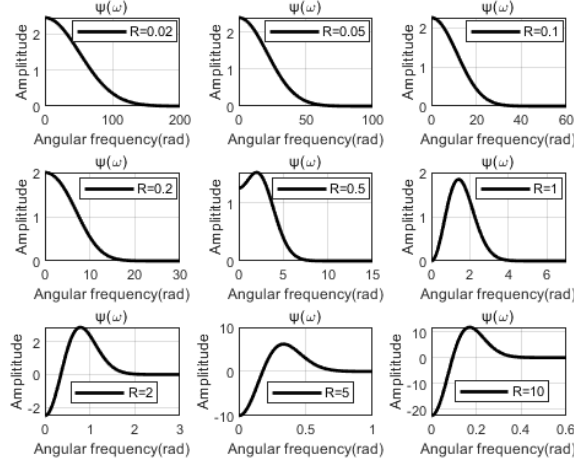


**Figure 3.** Spectrum of  $\psi(t)$  with different R value.

124 The I way mixed signal is

$$125 \quad X_I(t) = A\cos(2\pi f_0 t + \varphi(t)), t \geq 0. \quad (7)$$

126 The Taylor expansion of  $\varphi(t)$  at  $t = b$  is

$$127 \quad \varphi(t) = \varphi(b) + \varphi'(b)(t - b) + \dots \quad (8)$$

128 If the higher-order terms are ignored,  $\varphi(t)$  in the neighborhood of  $t = b$  can be expressed  
 129 as  $\varphi(t) = \varphi(b) + \varphi'(b)(t - b)$ . Therefore, equation (7) in the neighborhood of  $t = b$  is expressed  
 130 as

$$131 \quad X_I(t) = A\cos(2\pi f_0 t + \varphi(b) + \varphi'(b)(t - b)), t \in (b - \varepsilon, b + \varepsilon). \quad (9)$$

132 The Fourier transform of equation (9) is

$$133 \quad \begin{aligned} \widehat{X}_I(w) &= A\pi\delta(\varphi'(b) + 2f_0\pi - w)\exp(-ib\varphi'(b) + i\varphi(b)) \\ &+ A\pi\delta(\varphi'(b) + 2f_0\pi + w)\exp(ib\varphi'(b) - i\varphi(b)). \end{aligned} \quad (10)$$

134 The signal transformation of equation (9) is

$$135 \quad \begin{aligned} W_{If}(a, b) &= \int_{-\infty}^{\infty} X_I(t)\overline{\psi_{a,b}(t)}dt = \frac{1}{2\pi} \int_{-\infty}^{\infty} \widehat{X}_I(w)\overline{\widehat{\psi}_{a,b}(w)}dw \\ &= \frac{1}{2\pi} \int_{-\infty}^{\infty} \widehat{X}_I(w)\overline{\widehat{\psi}(a\omega)}e^{ibw}d\omega = B(a, b)\cos(\varphi(b) + 2bf_0\pi). \end{aligned} \quad (11)$$

136 In equation (11)  $B(a, b) = \sqrt{2\pi}A(1 - R + a^2(\varphi'(b) + 2f_0\pi)^2)R^3\exp(-\frac{1}{2}a^2(\varphi'(b) + 2f_0\pi)^2R^2)$   
 137 and overbar " - " denotes a complex conjugation.  $W_{If}(a, b)$  is the projection coefficients of  
 138  $X_I(t)$  on  $\psi_{a,b}(t)$ .

139 Similarly, for the Q way mixed signal

$$140 \quad X_Q(t) = A\sin(2\pi f_0 t + \varphi(t)), t \geq 0. \quad (12)$$

141 The signal transformation of  $X_Q(t)$  is

$$142 \quad W_{Qf}(a, b) = B(a, b)\sin(\varphi(b) + 2bf_0\pi). \quad (13)$$

143  $B(a, b)$  in equation (13) is the same with  $B(a, b)$  in equation (11).

144 The complex variable is constructed by using equations (11) and (13):

$$145 \quad Z_f(a, b) = W_{If}(a, b) + iW_{Qf}(a, b). \quad (14)$$

146 When  $a$  is determined,  $Z_f(a, b)$  degenerates into a complex variable  $Z_f(b)$  that is only  
147 related to the parameter  $b$ . Then,  $\varphi(b)$  is expressed as

$$148 \quad \varphi(b) = \arg(Z_f(b)) + 2bf_0\pi. \quad (15)$$

149 In this study, center frequency  $f_0 = 0Hz$ . Thus, equation (15) can be simplified to

$$150 \quad \varphi(b) = \arg(Z_f(b)). \quad (16)$$

151  $b$  is the translation parameter. If a series of time values are taken for  $b$ , the phase  
152 difference between the real and the reconstructed signals at each time can be obtained.  
153 The appropriate value of  $R$  in equation (3) is important. As shown in figure 3, the  $R$   
154 value determines the spectral characteristics of the basis function. In our application, the  
155 spectrum of the basis function should be characteristic of a low pass filter. Therefore,  $R$   
156 should be between  $0 < R < 1$ , with a bias towards small values.

157 From equation (6), it can be seen that the scale parameter  $a$  affects the scaling of the  
158 spectrum of  $\psi_{a,b}(t)$ , and the translation parameter  $b$  affects the shift of the spectrum of  
159  $\psi_{a,b}(t)$ .

160 Since the duration of the data used in each signal transformation is no more than 0.01  
161 seconds, it means that  $b \leq 0.01$ . Therefore, the influence of  $b$  on the spectrum of  $\psi_{a,b}(t)$  can  
162 be ignored. Thus, the spectrum of  $\psi_{a,b}(t)$  is mainly determined by  $a$  and  $R$ . For example,  
163 when  $R = 0.02$  and  $a = 50$  are selected, the spectrum of  $\psi_{a,b}(t)$  is characteristic of a low  
164 pass filter and also has an appropriate cut-off frequency. In fact, there are many other  
165 combinations of  $R$  and  $a$  that can also meet the application requirements, and parameters  
166 can be selected according to the characteristics of the actual signal.

167 In short, we define a new function family  $\psi_{a,b}(t)$ , then project two signals  $X_I(t)$  and  
168  $X_Q(t)$  onto  $\psi_{a,b}(t)$ . When  $a$  is a fixed value, the phase can be reconstructed by the projection  
169 coefficients of these two signals. The process of signal projection is essentially a signal  
170 filtering process, that's the reason why this algorithm proposed here is feasible.

### 171 **2.3 Data preprocessing by wavelet soft threshold denoising**

172 In practice, the mixed signals  $X_I(t)$  and  $X_Q(t)$  still contain a lot of noise after being  
173 processed by integrate/dump filter. Therefore, if the mixed signal is processed by signal  
174 transformation directly, the obtained phase is inaccurate. Therefore, the data preprocessing  
175 part must be included in the novel phase discrimination module. Wavelet soft threshold  
176 denoising is used in data preprocessing. The discrete Meyer wavelet (Dmey) is selected  
177 in this study. The level of wavelet decomposition  $n = [\log_2 N] - 1$ ,  $N$  is the number of  
178 data points which are used in each wavelet transform.  $[\log_2 N]$  represents taking the integer  
179 portion of  $\log_2 N$ . Then, the preprocessed data can be processed by phase discrimination  
180 based on signal transformation.

181 In the process of obtaining the phase of signal when using novel phase discriminator,  
182 two steps are included. The first step is preprocessing. Given the frequency of signal is small,  
183 a large amount of noise is eliminated by soft threshold denoising. The second step is to use  
184 new defined basis function to carry out signal transformation, because the selected basis  
185 function is characteristic of a low pass filter, so the noise is also removed in the process of  
186 phase extraction by signal transformation. Using an arctangent phase detector to calculate

187 the phase of signal with a duration of  $T$  is to directly calculate the argument angle of the  
 188 accumulated value of the data in that period. Compared with arctangent phase detector,  
 189 new phase detector optimizes signal denoising process.

### 190 3 Simulation

#### 191 3.1 Verify correctness of novel phase detector

192 The two signals are respectively expressed as  $X_I(t) = \cos(t + 1000t^2)$  and  $X_Q(t) =$   
 193  $\sin(t + 1000t^2)$ . This study sets the data sampling rate as  $F_s = 4MHz$ , time length as  
 194  $T = 1ms$ , and  $N = 50$ , where  $N$  means that the data with a duration of  $T$  is evenly divided  
 195 into  $N$  parts according to time and each part is accumulated into 1 point,  $N$  is also the  
 number of data points which is used in phase discrimination once. No noise is added.

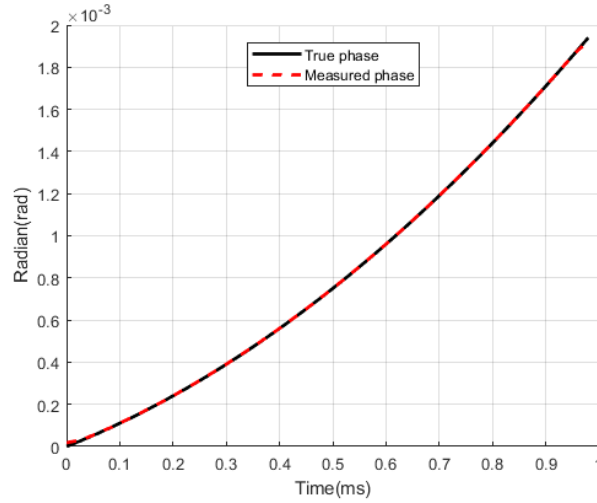


Figure 4. Set  $R = 0.02, a = 50$ , and the measured phase is shown.

196

197 Figure 4 shows that the phase of signal can be reconstructed accurately by using signal  
 198 transformation based on a new defined basis function. The average phase is obtained by  
 199 averaging the measured phase, then the average phase is used as the output of novel phase  
 200 detector and the input of loop filter.

#### 201 3.2 Validation of performance improvement

202 In this simulation, a novel phase detector is used to replace arctangent phase detector.  
 203 The weak signal is expressed as  $U_i(t) = \cos(2\pi ft) + n_0$ ,  $n_0$  represents noise. Set 23 sets  
 204 of signals with different SNR and the signal-to-noise ratios of these signals are respectively  
 205  $-55dB, -49dB, \dots, -33dB$ . SNR is calculated as  $10\log_{10} \frac{P_s}{P_n}$ , where  $P_s$  and  $P_n$  are the power  
 206 of the signal and the noise, respectively. For third-order PLL based on arctangent phase  
 207 detector and third-order PLL based on novel phase detector, 50 times of carrier tracking  
 208 experiments were conducted randomly for each group of signals with a set signal-to-noise  
 209 ratio, and tracking data for 30 seconds at a time. The residual frequency is obtained by  
 210 subtracting the measured frequency from the true frequency, and root mean square(RMS) is  
 211 calculated for the residual frequency of last 20 seconds. Frequency of signal is assumed to be  
 212 locked correctly when  $RMS < 1Hz$ , thus the probability that the frequency is locked correctly  
 213 was calculated. In this simulation, sampling rate is  $F_s = 4MHz$ , the first derivative of the  
 214 Doppler frequency is  $4Hz/s$  and initial frequency is  $1MHz$ . Make  $w_n$  gradually decrease

215 from 10 to 2 in the first 10 seconds. The time length of the data for phase discrimination  
 216 once is  $T = 10ms$ . The scale parameter is  $a = 1000$ ,  $R = 0.02$ , and  $N = 50$ . Because  
 217  $T = NT_0$ , then  $T_0 = 0.2ms$ . The estimated initial frequency is set to  $1000002Hz$  in each  
 218 carrier tracking experiment, so as to eliminate the effect of initial frequency estimation on  
 219 tracking results.

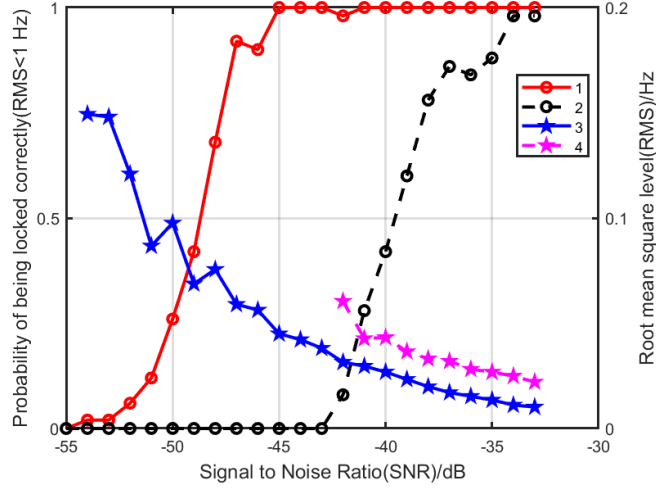


**Figure 5.** Label 1 and 2 represents Probability of being locked correctly obtained by PLL with novel phase detector and PLL with arctangent phase detector, respectively. Label 3 and 4 represents root mean square level(RMS) of 1 second Integral of residual frequency obtained by PLL with novel phase detector and PLL with arctangent phase detector, respectively. The first derivative of Doppler frequency is  $4Hz/s$ .

220 As is seen in figure 5, the weak-signal tracking ability of the PLL is greatly improved  
 221 when arctangent phase detector is replaced by novel phase detector. In addition, the accu-  
 222 racy of Doppler frequency measurement is also significantly improved.

223 Further, the first derivative of Doppler frequency is set as  $100Hz/s$ , and make  $w_n$   
 224 gradually decrease from 20 to 2 in the first 10 seconds. Another simulation result is shown  
 225 in figure 6. High-dynamic tracking capability and the robustness of PLL algorithm are  
 226 significantly improved by using novel phase detector.

227 When using the same hardware, the calculation amount of the two algorithms is com-  
 228 pared in Table 1. In simulation, we set sampling rate  $F_s = 4MHz$ , the duration of data is  
 229 1 second and  $N = 50$ .  $N$  is the number of data points which are used in each signal trans-  
 230 formation and calculation amount is positive correlated with  $N$ . But in our application,  
 231  $N = 50$  is a proper value, so let  $N$  be constant.

232 In addition,  $T$  is a flexible parameter, and the value of  $T$  affects the dynamic tracking  
 233 capability and weak signal tracking capability of PLL. When different values are taken for  $T$ ,  
 234 the comparisons between the two PLL algorithms are similar to the results shown in Figure  
 235 5 and Figure 6. Table 1 shows the calculation amount of the two kinds of PLL when different  
 236 values are taken for  $T$ . For data of every second, the number of phase discriminations is  
 237  $1/T$ . The smaller the  $T$  is, the more phase discriminations are required per second, and  
 238 the computation is also larger. The new algorithm is currently running in MATLAB, if the  
 239 code is rewritten by C programming language or some other programming language, then  
 240 computing time will be decrease significantly.

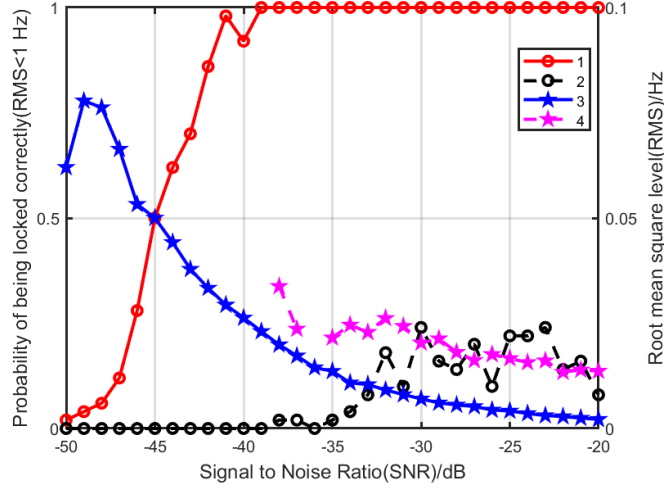


**Figure 6.** Label 1 and 2 represents Probability of being locked correctly obtained by PLL with novel phase detector and PLL with arctangent phase detector, respectively. Label 3 and 4 represents root mean square level(RMS) of 1 second Integral of residual frequency obtained by PLL with novel phase detector and PLL with arctangent phase detector, respectively. The first derivative of Doppler frequency is 100Hz/s.

**Table 1.** The amount of computation for both algorithms

Algorithm type	$T = 10ms$ computing time [s]	$T = 5ms$ computing time [s]	$T = 2ms$ computing time [s]	$T = 1ms$ computing time [s]
PLL with arctangent phase detector	0.81	0.78	0.78	0.80
PLL with novel phase detector	1.97	3.04	6.26	11.62

### 241 3.3 High-dynamic and extremely weak signal processing

242 Consider carrier tracking in the entry, descent, and landing (EDL) phase of Mars prober  
 243 is most challenging. So large dynamic is set in simulation data, figure 7 shows Doppler  
 244 shift and the first derivative of Doppler shift of simulation data. The maximum second  
 245 derivative of Doppler shift is  $540Hz/s^2$ , and the maximum first derivative of Doppler shift  
 246 is  $3612.1Hz/s$ . The sampling rate of simulation data is 4MHz, the signal-to-noise ratio(SNR)  
 247 is set to  $-40dB$ .  $T$  is 2.5ms. The loop noise bandwidth is set to  $16.67Hz(w_n = 20)$ . Other  
 248 settings are the same as above.

249 Most of the signal is drowned out by noise, including the first second data. Therefore,  
 250 the strategy for rough estimation of initial frequency is to compensate a series of phase  
 251 values for the first second data and then the frequency index corresponding to maximum  
 252 amplitude is detected. The obtained frequency index can be used for initialization of PLL.

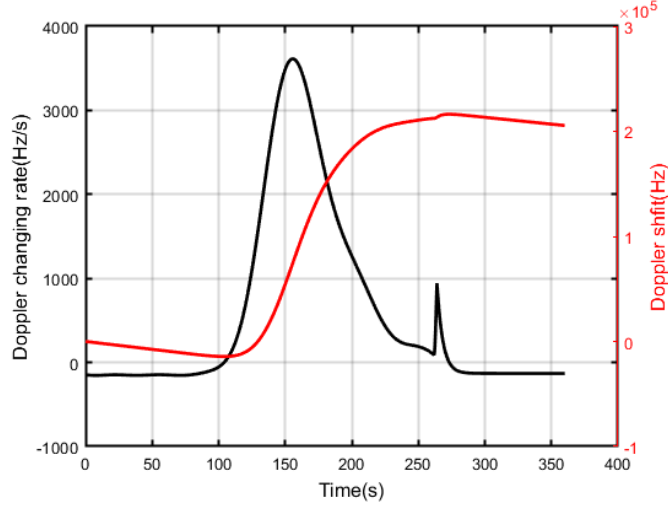


**Figure 7.** The Doppler shift and Doppler changing rate of simulation data.

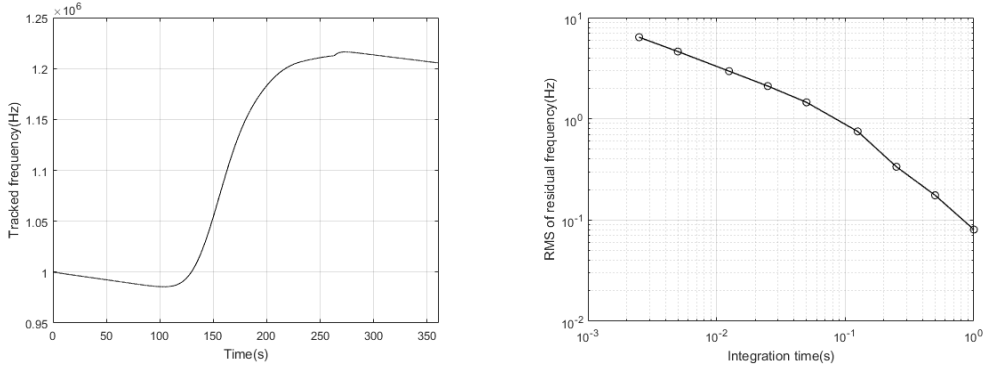


**Figure 8.** (a) The recovered frequency of simulation data; (b) Tracking accuracy of Doppler frequency at different integration times.

#### 253 4 Actual data processing

254 When processing actual data, the loop noise bandwidth is set to  $8.33Hz(w_n = 10)$ .  
 255 Actual data consists of four channels of signals which received by UR telescope during  
 256 the Chang'e-3 landing phase. Figure 9 shows that the actual data processing results also  
 257 demonstrated the excellent performance of new method and this method will be very useful  
 258 in deep space exploration.

#### 259 5 Conclusion

260 This study proposes a novel phase detector to replace the arctangent phase detector.  
 261 The new phase discriminator greatly improves performance of PLL, including the weak-  
 262 signal tracking ability, tracking accuracy and high-dynamic tracking capability. The simu-  
 263 lation and actual data processing results demonstrate the effectiveness of this new proposed  
 264 method.

265 Data preprocessing in the new phase detector is very important. Data preprocessing  
 266 can effectively remove noise, an indispensable part of the whole new phase detector.

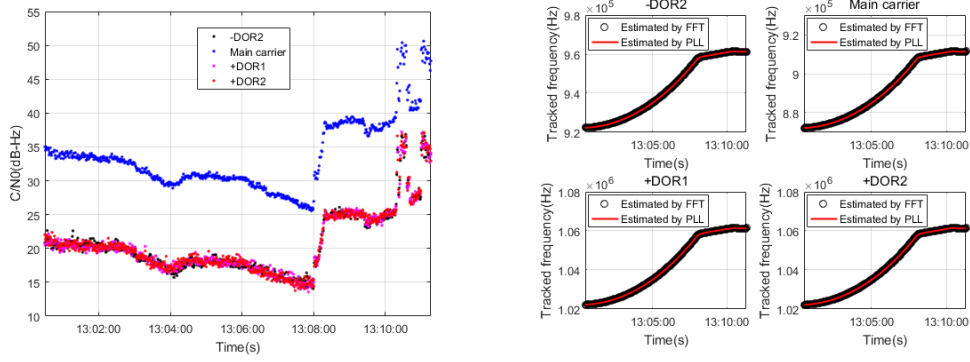


**Figure 9.** (a) Estimation of the carrier-to-noise ratio of data received by UR telescope during the Chang'e-3 landing phase; (b) The recovered frequency of actual data.

267 When proper  $R$  and  $a$  values are selected, the spectrum of  $\psi_{a,b}(t)$  should be character-  
 268 istic of a low pass filter and also has an appropriate cut-off frequency.

269 There are two reasons not to use traditional wavelets. First, because admissibility  
 270 condition should be satisfied, the spectrum of wavelets always have the characteristics of a  
 271 band-pass filter, not a low-pass filter. Second, the phase of the signal may not be obtained  
 272 by using the coefficients of wavelet transform.

273 The correct phase detection range of the new phase detector is  $\pm\pi$ . The reconstructed  
 274 phase needs to remove the phase value of an integer multiple of  $2\pi$  to ensure that the  
 275 phase difference between the real and the reconstructed signals does not exceed the phase  
 276 discrimination range of the new phase detector. In this way, the divergence of the phase  
 277 discrimination error can be limited.

## 278 Acknowledgments

279 The present study is supported by the National Natural Science Foundation of China (Grant  
 280 Nos. 11773060, 11973074, U1831137, and 11703070), National Key Basic Research and  
 281 Development Program (Grant No. 2018YFA0404702), Shanghai Key Laboratory of Space  
 282 Navigation and Positioning (Grant No. 3912DZ227330001), and the Key Laboratory for  
 283 Radio Astronomy of CAS. Data of Change-3 for this research are not publicly available  
 284 and stored in very long baseline interferometry (VLBI) data processing center of Chinese  
 285 Academy of Sciences in Shanghai. If someone needs any data of this article, please contact  
 286 the author via email: dengtao@shao.ac.cn.

## 287 References

- 288 Cattivelli, F. S., Estabrook, P., Satorius, E. H., & Sayed, A. H. (2008). Carrier recovery  
 289 enhancement for maximum-likelihood doppler shift estimation in mars exploration  
 290 missions. *IEEE Journal of Selected Topics in Signal Processing*, 2(5), 658-669.
- 291 Hao, W., Dong, G., Li, H., Wang, H., Fan, M., Zhou, h., & Xu, D. (2018). Key technolo-  
 292 gies for communications in mars entry descent and landing. *Journal of Deep Space*  
 293 *Exploration*, 426-434.
- 294 Li, Y., Xu, X., & Zhang, T. (2011). Improving tracking performance of pll based on  
 295 wavelet packet de-noising technology. In S. Lin & X. Huang (Eds.), *Advances in*  
 296 *computer science, environment, ecoinformatics, and education* (pp. 449-456). Berlin,  
 297 Heidelberg: Springer Berlin Heidelberg.
- 298 Lopes, C. G., Satorius, E., & Sayed, A. H. (2006). Adaptive carrier tracking for direct-to-

- 299 earth mars communications. In *2006 fortieth asilomar conference on signals, systems*  
 300 *and computers* (p. 1042-1046).
- 301 Mao, w.-l., & Chen, A.-B. (2008, 03). Mobile gps carrier phase tracking using a novel  
 302 intelligent dual-loop receiver. *Int. J. Satellite Communications Networking*, *26*, 119-  
 303 139. doi: 10.1002/sat.898
- 304 Pengyue, S., Xiaomei, T., Yangbo, H., Huaming, C., & Guangfu, S. (2016). Adaptive wavelet  
 305 denoising unscented kalman filter for beidou signal carrier tracking under ionospheric  
 306 scintillation conditions. *Journal of Applied Remote Sensing*, *10*(4).
- 307 Ruan, H., Zhang, L., Luo, Y., & Long, T. (2017). Gnss carrier phase tracking with discrete  
 308 wavelet transform filtering under ionospheric scintillation. *IEEE Communications*  
 309 *Letters*, *21*(2), 394-397.
- 310 Satorius, E., Estabrook, P., Wilson, J., & Fort, D. (2003, 01). Direct-to-earth communi-  
 311 cations and signal processing for mars exploration rover entry, descent, and landing.  
 312 *Interplanetary Network Progress Report*, 1-.
- 313 Soriano, M., Finley, S., Jongeling, A., Fort, D., Goodhart, C., Rogstad, D., & Navarro, R.  
 314 (2012, 03). Spacecraft-to-earth communications for juno and mars science laboratory  
 315 critical events.  
 316 doi: 10.1109/AERO.2012.6187098
- 317 Sun, P., Tang, X., Huang, Y., & Sun, G. (2017). Wavelet de-noising kalman filter-based  
 318 global navigation satellite system carrier tracking in the presence of ionospheric scin-  
 319 tillation. *IET Radar, Sonar Navigation*, *11*(2), 226-234.
- 320 Tian, T., Cui, C., & Cheng, L. (2016). Design and simulation of third order phase-locked  
 321 loop in high-dynamic applications. *Space Electronic Technology*, *13*(4), 57-60.
- 322 Vil-Valls, J., Closas, P., & Fernandez-Prades, C. (2015). On the identifiability of noise  
 323 statistics and adaptive kf design for robust gnss carrier tracking. In *2015 ieee aerospace*  
 324 *conference* (p. 1-10).
- 325 Vila-Valls, J., Closas, P., Navarro, M., & Fernandez-Prades, C. (2017). Are plls dead? a  
 326 tutorial on kalman filter-based techniques for digital carrier synchronization. *IEEE*  
 327 *Aerospace and Electronic Systems Magazine*, *32*(7), 28-45.
- 328 Won, J. (2014). A novel adaptive digital phase-lock-loop for modern digital gnss receivers.  
 329 *IEEE Communications Letters*, *18*(1), 46-49.
- 330 Won, J., Pany, T., & Eissfeller, B. (2012). Characteristics of kalman filters for gnss signal  
 331 tracking loop. *IEEE Transactions on Aerospace and Electronic Systems*, *48*(4), 3671-  
 332 3681.
- 333 Zhong, J., & Weng, J. (2005, Oct). Phase retrieval of optical fringe patterns from the  
 334 ridge of a wavelet transform. *Opt. Lett.*, *30*(19), 2560-2562. Retrieved from [http://](http://ol.osa.org/abstract.cfm?URI=ol-30-19-2560)  
 335 [ol.osa.org/abstract.cfm?URI=ol-30-19-2560](http://ol.osa.org/abstract.cfm?URI=ol-30-19-2560) doi: 10.1364/OL.30.002560